PCCP

Accepted Manuscript

ROYAL SOCIETY OF CHEMISTRY

www.rsc.org/pccp

Designing flexible energy and memory storage materials using cellulose modified graphene oxide nanocomposites

Abdullahil Kafy, Kishor Kumar Sadasivuni, Hyun-Chan Kim, Asma Akther, Jaehwan Kim*

Center for EAPap Actuator, Dept. of Mechanical Engineering, Inha University, 253 Yonghyun-Dong, Nam-Ku, Incheon 402-751, South Korea

Corresponding Author

Tel.: +82 32 860 7326; Fax: +82 32 832 7325

E-mail: jaehwan@inha.ac.kr (Jaehwan Kim)

Abstract

The demand of flexible energy storage devices is ever increasing and several polymer nanocomposites are widely used to fabricate them. Here we present a cellulose based nanocomposite by incorporating graphene oxide (GO) nanoplatelets modified with hexamethylene diisocyanate grafting agent useful for such versatile applications. The simple method of casting/solvent evaporation is applied to prepare the nanocomposites and GO dispersion in the cellulose matrix was analyzed by Fourier transform infrared spectroscopy, X-ray diffraction studies and scanning electron microscopy. The dielectric and ferroelectric properties of the eco-friendly samples were checked with temperature and voltage variations, which can attribute to flexible energy and memory storage properties. Thus the cellulose modified GO nanocomposite has turned to be environmentally stable and excellent next generation material for energy storage and electronic devices.

Keywords- Energy and memory storage; Grafting; Cellulose; Graphene oxide; Flexible electronics; Ferroelectric; Dielectric.

Introduction

The biopolymer cellulose is an inexhaustible source of raw material for numerous eco-friendly devices and is the most abundant natural polymer on the earth [1]. The various applications of cellulose based composites include coatings, laminates, optical films, pharmaceuticals, food and textiles and so on [2-4]. Cellulose forms the promising base material for flexible electronics due to its low cost, light-weight, relatively high thermo stabilization, high sorption capacity, alterable optical appearance and biocompatibility [5, 6]. The basic structure of this material has the advantage of forming many strong interactions with the filler particles and this is the reason for thousands of bio products based on it.

Nowadays, energy storage devices are essential for many portable devices and eco-friendly materials replace the conventional acid battery metallic storage devices requiring more recharge time, acid utilization and less abundance. The current main strategy to fabricate innovative and advanced materials from naturally available materials mainly targets the most abundant cellulose [10, 11]. Numerous polymeric nanocomposites other than cellulose are also being explored in the field of flexible and wearable electronics to fabricate energy storage devices [7–9], where the flexible capacitors should be specially mentioned in modern applications [12-13]. The carbon fibers, carbon nanotubes and graphene derivatives are widely used as filler materials for energy devices (as free-standing and flexible capacitors) due to their favorable flexibility [10, 14-18]. Of the several nanocarbons, two dimensional graphene nanosheets is promising due to its ultra-high specific surface area (~2,630 m^2/g) and excellent electronic properties and applications [19, 20]. It is reported that the polar graphitic derivatives such as graphene oxide (GO) filled cellulose nanocomposites possess very high mechanical,

thermal and gas permeability properties [21-23]. However the low conductivity of GOs does not allow the formation of electronic devices and reduced GOs are largely used for those purposes.

The presence of large number of hydroxyl groups of cellulose along the GO skeleton causes the formation of comprehensive networks of intra- and inter-molecular hydrogen bonds with the cellulose matrix thus forming the two -crystalline and amorphous- structural regions in the same polymer [24]. When the polar fillers are uniformly bonded with the neat cellulose, flexible biomaterials result [25-27]. But the facile aggregation of graphene during synthesis degrades the material performance composed of graphene and reduced GO and lower performance of those composites is often reported. This fact can be minimized by modifying the GO sheets with proper functional groups so as to maintain strong interactions with the cellulose matrix.

In this work, we used grafting method to bond cellulose with GOs by using diisocynate grafting method. We have experimentally demonstrated the scientific significance of dielectric and ferroelectric properties within the cellulose-grafted-GO (CFG) nanocomposites in order to apply in energy storage and electronic devices. The CFG nanocomposites have ferroelectric behavior associated with a built-in polarization that is switchable and vary with temperature. The energy and memory storage properties are correlated with the morphology-structure relationship of the obtained CFG nanocomposites by means of Fourier transformation infrared spectroscopy (FTIR), X-ray diffraction (XRD) and scanning electron microscopy (SEM) studies.

Experimental Details

Materials

Cotton pulp of 98% purity and degree of polymerization 4500 was obtained from Buckeye Technology, USA. Natural flake graphite, and other reagents such as Hexamethylene-1,6-diisocyanate (HMDI), Dimethyl Acetamide (DMAc), Lithium Chloride (LiCl), Sulfuric Acid (H_2SO_4), Nitric Acid (HNO_3), Hydrochloric acid (HCl), Potassium permanganate ($KMnO_4$) and 30% Hydrogen Peroxide (H_2O_2) solution were procured from Sigma-Aldrich. The 99.5% isopropyl alcohol was purchased from Daejung, South Korea.

Sample preparation

Cellulose solution was prepared using the common DMAc/LiCl system [1]. The cotton pulp and LiCl were dried in the oven air at 100 °C to remove water molecules prior to this. The mixture of 2/8/90 cotton pulp, LiCl and anhydrous DMAc were heated at 155 °C by mechanical stirring for 4 h in order to obtain a viscous solution and centrifuged at 11000 rpm to eliminate the undissolved cellulose fibers. The GOs were synthesized by the improved graphene oxide method [28], the AFM and TEM images of which are given in supplementary information (Figure S1). Functionalization of GOs was done by treating with HMDI. For this purpose, 20 mg of GO was first dispersed in 20 ml of anhydrous DMAc for 30 minutes, thereafter adding the 0.2 g of HMDI by stirring at 110 °C for 3 h. To this mixture cellulose dissolved DMAc solution was added and mechanically stirred for 3 more hours. The schematic of the reaction mechanism involved between GOs and cellulose by the HDMI agent is represented in Figure 1. The possible mechanism could be happened by the reaction of initially added HMDI having isocyanate group with hydroxyl (or) epoxy (or) carboxyl groups on GO instantly at mentioned temperature and the

other end of HMDI isocyanate group reacting with subsequently added hydroxyl groups of cellulose or GO [10].

Finally the composite solution was casted on a glass plate using doctor blade and cured using deionized water for 3 h. This slow curing process prevents aggregation of GOs and eliminates the remnants LiCl and DMAc. Finally the cured wet nanocomposite was rinsed in two different deionized water baths and dried in a vacuum oven at 60 °C. Table 1 shows the various nanocomposite samples used for the analyses.

Table1: Comparison of different properties with the increment of filler in cellulose

Notation of Samples	Weight % of Filler	Young's Modulus GPa	Dielectric Constant ε′ at 20 Hz	Transmittance %
Cellulose	0	2.37	16	85.97
CFG0.5	0.5	3.18	304	68.61
CFG1	1	3.31	1052	65.13
CFG2	2	3.53	2411	58.01
CFG3	3	3.86	3044	34.20

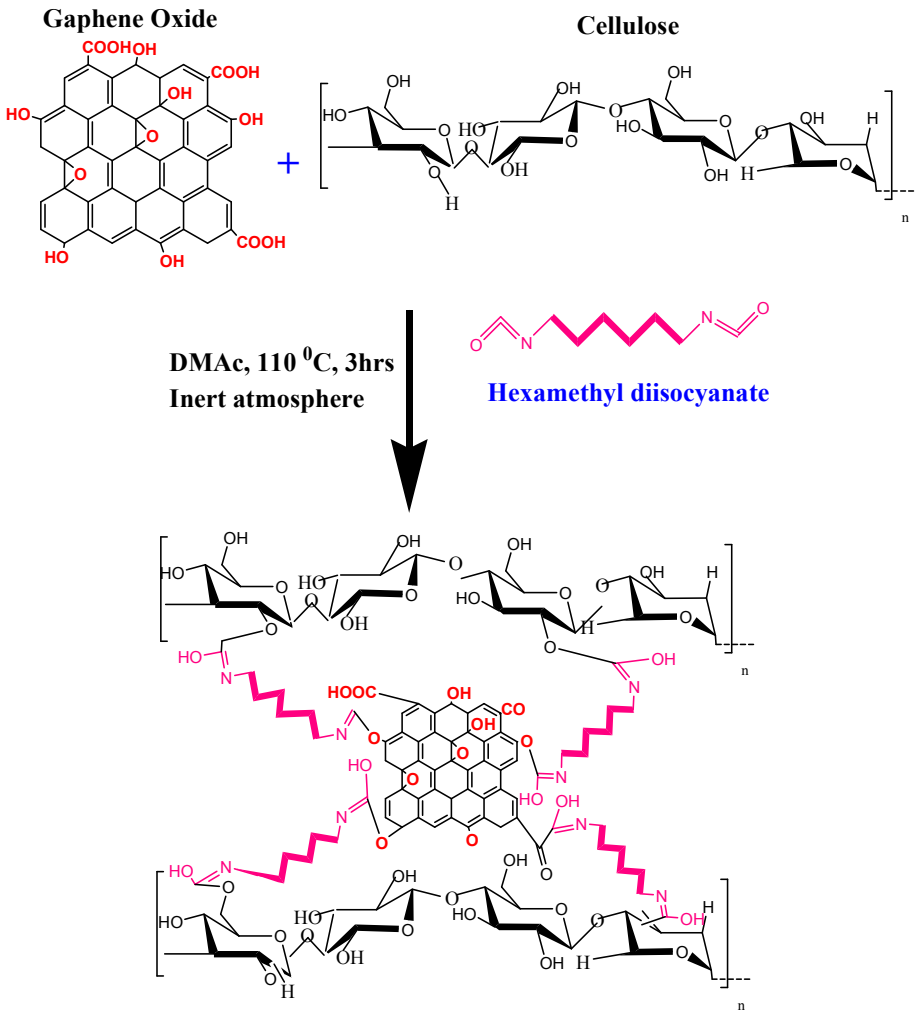

Figure 1: Reaction mechanism of cellulose with GOs grafted using hexamethylene diisocyanate.

Characterization

FE-SEM images of the sample films were taken with JEOL JSM-6400F microscope to study the sample morphology. The samples were prepared by coating platinum layer using ion sputter (EMITECH, K575X). The FTIR spectra (Bruker Optics, Billerica, MA) were obtained in the range of 500–4000 cm^{-1} by averaging 16 scans (Resolution was 4 cm^{-1}) at 1 min intervals to minimize the effects of dynamic scanning and to qualitatively demonstrate covalent grafting of GOs to cellulose. XRD patterns were checked with a thin film X-ray diffractometer using CuKα

target radiation at 40 kV and 50 mA, at a scanning rate of 0.015°/min. The diffraction angle was varied from 5 to 40°. Optical transmittance of the samples was studied using a UV-visible spectrophotometer. For this the spectra of the films in the range of 200-800 nm wavelengths were recorded with a Hewlett Packard (8452A) diode array.

The variation in dielectric constant of the cellulose matrix and its nanocomposites between 20 - 10 kHz frequency were monitored using an LCR meter (HP 4284A). Measurements were done at 25 °C temperature, 25% relative humidity and at 1 V. The ferroelectric behavior of samples (Au–sample film– Au in thickness direction) was characterized by electric fields ranging from −3 to 3 $kVcm^{-1}$ with a 1 Hz saw tooth wave using a ferroelectric tester (Radiant Technology Premier II).

Results and discussion

Morphology and structure relationship

It is rather important to study the morphology and structure of the nanocomposite samples in order to explain its properties. The cross-sectional FE-SEM images are given in Figure 2, which show the morphological changes induced by GOs on cellulose. No agglomeration of GOs was observed in the CFG nanocomposites as illustrated in the images. Cellulose possesses rough morphology (Figure 2a) and the roughness reduced upon the addition of GOs. The very smooth and well bind surface in the nanocomposites indicates good reinforcement between GO filler and cellulose matrix (Figure 2b, 2c) as well as good GO dispersion. The absence of aggregated GO platelets was observed in cellulose even at 3% loading.

The optical properties of the cellulose and its nanocomposite change with the increment of GO content in the nanocomposites. As given in Figure S2, a transparency decrease with increase of the GOs weight percent was observed.

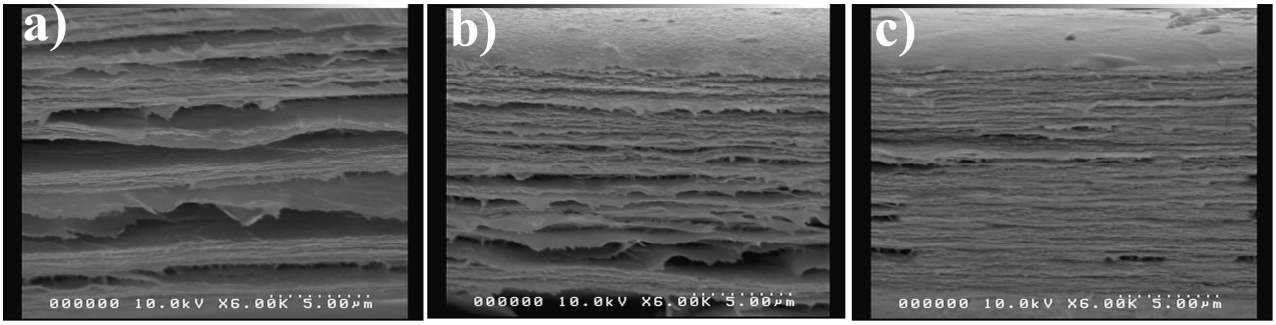

Figure 2: SEM cross section image of a) cellulose b) CFG1 c) CFG3

The structural composition was studied here with the help of FTIR and XRD techniques. To investigate the successful functionalization of GO, FTIR of GO, HMDI, cellulose and its nanocomposites were taken as shown in Figure 3. GO shows the C–O stretching vibration at 1209 cm^{-1}, O–H stretching at 3459 cm^{-1}, C-O at 1060 cm^{-1} and C=O stretching at 1711 cm^{-1} (Figure 3a). From the characteristic FTIR spectra of cellulose nanocomposites (Figure 3b) bands around 3418, 1607 and 1375cm^{-1} respectively corresponds to the O-H stretching, carboxyl bending and C–O–H bond vibrations of cellulose [23]. In addition, bands at 1137 cm^{-1} are due to the C-H bending modes and the peaks at 2932 cm^{-1} denote the characteristic C-H stretching of -CH_2 group (from cellulose). The appearance of new band at 1565 cm^{-1} originating from either amide or carbamate esters corresponds to the coupling of C-N stretching vibration with the CHN deformation vibration which ensures the functionalization of HMDI between GO and cellulose [10].

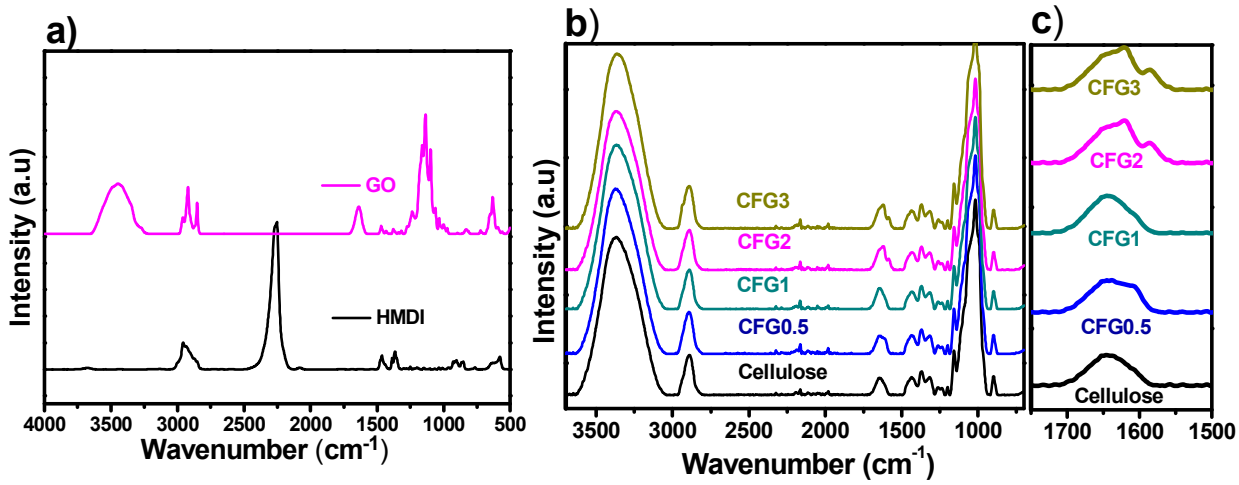

Figure 3: FTIR Spectra of a) HMDI and GO, cellulose and CFG nanocomposites with different weight percentage with b) 3700- 500 cm^{-1}c) 1750-1500cm^{-1}

In the nanocomposite containing 0.5 wt% of GO, FTIR does not show any absorption peaks as the amount of GO is very low. More importantly, the asymmetric NCO stretching vibration of the HMDI at 2275-2263 cm^{-1} is not seen in the spectra of the nanocomposite. Note that these peaks are visible starting from the nanocomposite containing 2 wt% GO. Based on all these facts, a mechanism proposed in Figure 1 is expected to be happening in the nanocomposites via the development of strong chemical interaction.

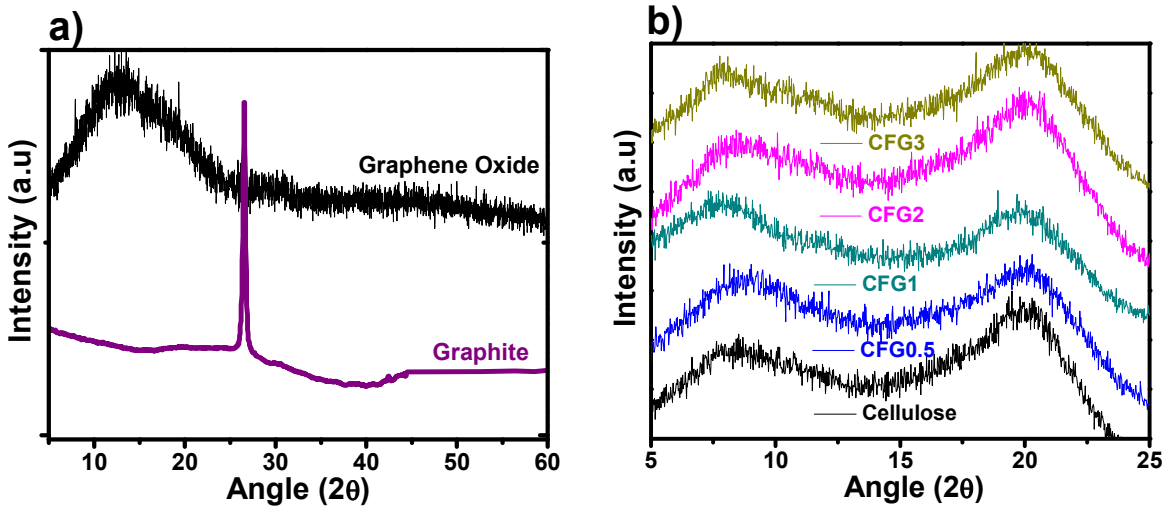

Figure 4: XRD spectra of a) GO and graphite b) CFG nanocomposites and cellulose.

The XRD patterns of GO, graphite, cellulose and its nanocomposites shown in Figure 4 furnish interesting facts about dispersion of filler and the sample morphology. The peak marked in Figure 4a corresponds to the (0 0 2) reflection in graphite and its derivative (GO). The diffraction peak of pristine graphite at around 2θ=26.52° determines an interlayer distance of 3.354 Å. In the case of GO, the peak corresponds to d value of 8.0854 Å [26]. Figure 4b gives information about the crystalline structure of the nanocomposites and dispersion of GOs in cellulose. The broad diffraction peak at 19° indicates the partly crystalline nature of the cellulose. Overall, the XRD spectra of all nanocomposites are similar to cellulose since the GO dispersed well. Moreover, the peak corresponding to GO disappeared in the XRD spectra of CFG nanocomposites confirming the exfoliation of the layered GO nanosheets in the cellulose matrix and this does not have any significant effect on crystallinity.

Dielectric/Energy storage property

In order to check the energy storage capability of the material the dielectric response of the samples, the dielectric constant ε' and dielectric loss (tan δ) at 20-10,000 Hz, 25 °C temperature, 25% relative humidity and at 1 V are checked as plotted in Figure 5. The ε' of a dielectric polymer depends on the amount of mobile (polarizable) electrical charges in it and the degree of mobility of these charges. The ε′ of CFG3 showed about 290 times enhancement (ε′=3,044) than that of the neat cellulose (ε′=16) and compared to the other nanocomposites CFG0.5 (ε′= 304), CFG1 (ε′=1,052) and CFG2 (ε′=2,411). These ε′ values are found at 20 Hz. The comparison of the dielectric properties between the cellulose and its nanocomposites at 20 Hz are given in Table 1. It was shown that under low frequency, the ε′ increases with the increasing wt% of GO. A similar report was done by Milan et al., in which they modified the graphene covalently using 6-amino-4-hydroxy-2-naphthalenesulfonic acid for energy storage application [29]. Since a lot of dipoles were obtained due to the special polarization structure of cellulose nanocomposite of strong polarity, large values of ε′ with low dielectric loss was observed [30, 31].

The dielectric measurements also show that the increase in GO concentration increases ε' (Figure 5). Upon comparing the permittivity, cellulose nanocomposite possesses enhanced values than the neat due to the motion of free charge carriers at interfacial polarization. According to Maxwell-Wagner-Sillars (MWS) process polymer-filler interfacial (like donor-acceptor complexes) interaction is necessary to get changes in the dielectric properties of nanocomposites. The huge interfacial area of nanocomposites provides numerous sites for the reinforced MWS effect as well [32]. In the MWS effect, when a current flows across the two-material dielectric

interfaces, charges accumulate at the interface with different relaxation time ($\tau = \varepsilon/\sigma$, where ε is the dielectric permittivity and σ is the conductivity). This is possible by the presence of moderate number of oxide functionalities (charge centers) and conjugation (carrier centers) on the GO sheet surface which forms a capacitor network to store energy [23]. From Figure 5, it is clear that the ε' has two different regions: the first, representing an exponential increase at a low frequency, below 100 Hz and the second showing a linear relation between the frequency and the ε' in the range of high frequency, above 100 Hz. The first term is related to the rotational movement of functional groups in the samples [33], which can be decelerated at high frequency. The second one is from the natural behavior of the existing functional in the nanocomposites, which cannot move easily at higher frequency [34].

The ε' of the cellulose nanocomposites increases with CFG filler loading [35, 4] as well (Figure 5). Since ε' at higher frequencies (kHz) mainly originates from the electrical conduction and dipolar polarization, the decrease in its value in the nanocomposites should be mainly attributed to the highly restricted polymer chain motion. Considering the nanocomposites with high ε' and low dielectric loss as more attractive for practical applications, the CFG3 shows superior property (Figure 5b). The losses occurring at low frequencies are primarily due to quasi DC conduction as caused by the percolation effect. In comparison with the cellulose matrix, the nanocomposites also exhibit a relatively 5 times dielectric loss. At frequencies from 10^2 to 10^4 Hz, tan δ decreases due to the failure of the induced charges to follow the reversing field, thus leading to reduced electronic oscillations, consistent with the aforementioned analysis of the cellulose nanocomposites.

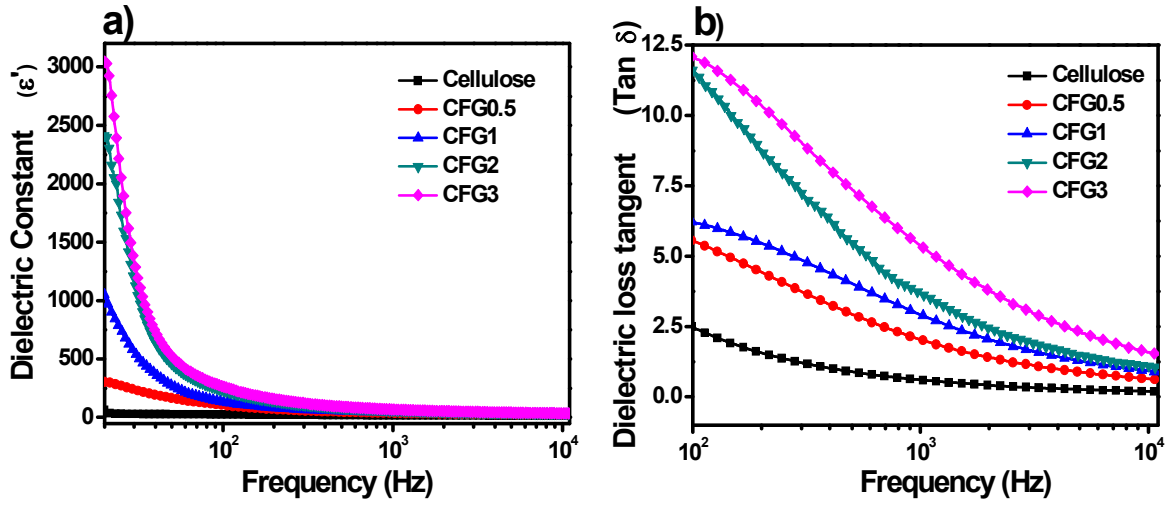

Figure 5: Variation of a) ε′ and b) tan δ of cellulose and its nanocomposites with frequency (At 1V, 25% R_H and 25 °C)

Influence of temperature on the dielectric behavior

The dielectric performance of a material is better understood by studying its temperature and voltage dependence. Figure 6 shows the measured dielectric behavior of the cellulose and its nanocomposites as a function temperature and voltage. Figure 6a illustrates the dielectric constant, ε′ vs voltage curves of the cellulose nanocomposites measured at 1 kHz. With applied voltage, the maximum dielectric constant observed was near -1 V and this study confirms the depletion of charge in the cellulose nanocomposites. Under high voltage, the electrons move easily towards the opposite electrode while they start to be stored as the applied voltage decreases. The trapped charges increase until the opposite applied field becomes high enough to activate the trapped electrons to escape from the trap sites. Over the activating level of the applied field, the dielectric constant, ε′ decreases due to the movement of electrons escaping

from the trap sites towards the electrode. A similar observation is also seen in the opposite case. Thus, it is considered that the functional groups inside the samples play an important role in governing the voltage effect behavior [36]. The dielectric behavior of the nanocomposites is attributed to the increase in charge density and significant improvement in the charge transport in the cellulose matrix. The influence of voltage is more pronounced in the CFG nanocomposites than the neat cellulose due to the increase in rate of rotation of dipolar molecules.

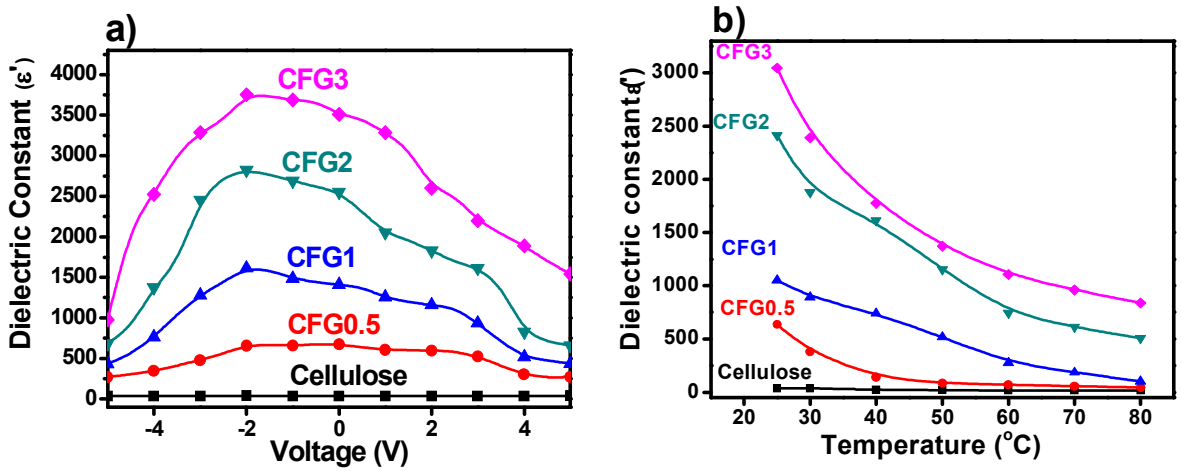

Figure 6: Variation of dielectric properties of CFG nanocomposites with (a) voltage and (b) temperature.

The ε′ of the CFG nanocomposites decreases as the temperature increases (Figure 6b). It is clear from all dielectric observation that this particular property is related to the decrease in interfacial polarization and humidity (water molecules) which results in lower ε′ [36]. Compared with cellulose, the CFG nanocomposites show a strong temperature-dependent dielectric response, particularly at lower frequencies. The introduction of the GO flakes again results in much stronger temperature-dependent dielectric response and the nanocomposites' dielectric behavior

is similar to that of polar polymers such as polyamide. At high temperatures, the mobility of charge carriers and the rotation of dipoles would be significantly reduced and the interfacial polarization enhanced. Consequently the nanocomposites exhibit lower ε′ at high temperatures [37]. At a fixed frequency, ε′ decreases with the temperature increase, attributed to the greater restriction of movement of dipole molecular chain of cellulose at high temperature. As the temperature increases, the dipoles are comparatively restricted and reluctant to the applied electric field. Finally, excellent dielectric response of the CFG nanocomposites was identified at low frequency, low temperatures and low voltage. The lower dielectric constant at higher voltage causes non linearity in low-distortion filters and other analog applications.

Memory storage behaviour

The memory storage capability of the sample films were identified by means of measured polarization (P) as a function of electric field (E) i.e. P-E hysteresis curve. Figure 7 gives the P-E hysteresis loops for cellulose and its CFG nanocomposites at room temperature under 1 Hz. Generally a P-E loop for a device is a plot of the charge or polarization, against the applied field at a given frequency and the Log P-E variation is given as supplementary information (Figure S3). The P-E loop as shown in Figure 7 is the combination of ideal linear capacitor and resistor. It is observed that the area of the hysteresis loop of all samples have significant improvement. With GO addition, the shape of the hysteresis loops changes (Figure S4) as the polarization hysteresis is increased with increasing GO content. The shape of the loop assumes a more elliptic form as the temperature increases, which means that resistance element of the nanocomposite increases more than the capacitance part (Figure S4).

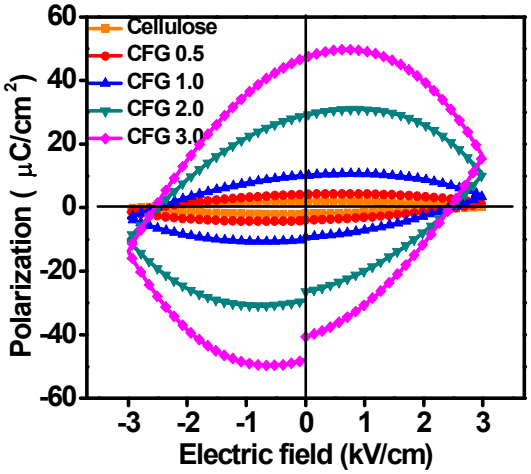

Figure 7: Variation of ferroelectric properties of CFG nanocomposites and cellulose at 25% R_H and 35 °C

The remnant polarization (P_r) and maximum polarization increase gradually with the filler concentration. It seemed that the nanocomposites were more easily to be polarized than cellulose, i.e., in the same field strength, the polarization effect for nanocomposite was easier than the one for neat cellulose [36, 38, 39]. Table 2 represents the summary of the P-E measurement, i.e., the temperature dependences of the coercive field (E_c) and P_r in which they are defined by the half width of the loop at P=0 and E=0, respectively. E_{max} and E_{min} indicate the range of applied E field. The GO is polar filler having dipolar alignment and reorientation, as well as increased polarization level and energy barrier. Thus, the addition of GO increases the relative concentration of dipole moment in the samples and the ability of reorientation of the dipoles along the field direction results in the increase of polarization effect. This behavior is in

accordance with the results based on graphene-based Fe-FET memory devices fabricated on inorganic ferroelectrics [40, 41].

Table 2: Summary results of polarization measurements. GO and P-GO are measured using PMF1011-278 ferroelectric tester with standard bipolar system (Precision LC Radiant Technology) keeping measurement parameters remains same. [Area = 2.25 cm^2; Thickness= 20 µm; Hysteresis Period = 1000 ms; Preset delay = 10 ms)].

Sample	Applied E Field (kV/cm)		Coercive Field (kV/cm)		Polarization (µC/cm^2)		
	E_{max}	E_{min}	$+E_c$	$-E_c$	P_{max}	$+P_r$	$-P_r$
Cellulose	2	-2	1.772	-1.900	1.275	1.272	-1.052
	3	-3	2.711	-2.801	1.975	1.967	-1.648
	4	-4	3.633	-3.776	2.623	2.601	-2.225
CFG 0.5	2	-2	1.661	-1.586	2.208	2.045	-1.937
	3	-3	2.567	-2.487	3.791	3.639	-3.432
	4	-4	3.505	-3.446	5.648	5.478	-5.006
CFG 1	2	-2	1.607	-1.586	5.702	5.361	-4.745
	3	-3	2.471	-2.508	9.726	9.196	-7.992
	4	-4	3.430	-3.484	13.960	13.450	-11.729
CFG 2	2	-2	1.585	-1.623	17.236	15.983	-13.781
	3	-3	2.454	-2.545	26.721	25.573	-22.093
	4	-4	3.452	-3.499	39.390	37.863	-34.879
CFG 3	2	-2	1.569	-1.639	34.879	32.819	-27.890
	3	-3	2.396	-2.524	53.669	51.213	-44.120
	4	-4	3.302	-3.467	72.310	69.486	-66.349

Influence of temperature on the ferroelectric properties

Temperature studies on the polarization as a function of the electric field are necessary for the detailed understanding of the polarization behavior of the samples. Figure 8a represents the variation of ferroelectric data from 25 to 80 °C. A close similarity is observed for the results with the temperature dependent dielectric behavior shown in Figure 6b. The maximum

polarization under constant electric fields was observed at lower temperatures and the polarization value decreases in a certain electric field as the temperature increases. Note that the polarization at 35 °C is about 30 times larger than that of the value near 80 °C.

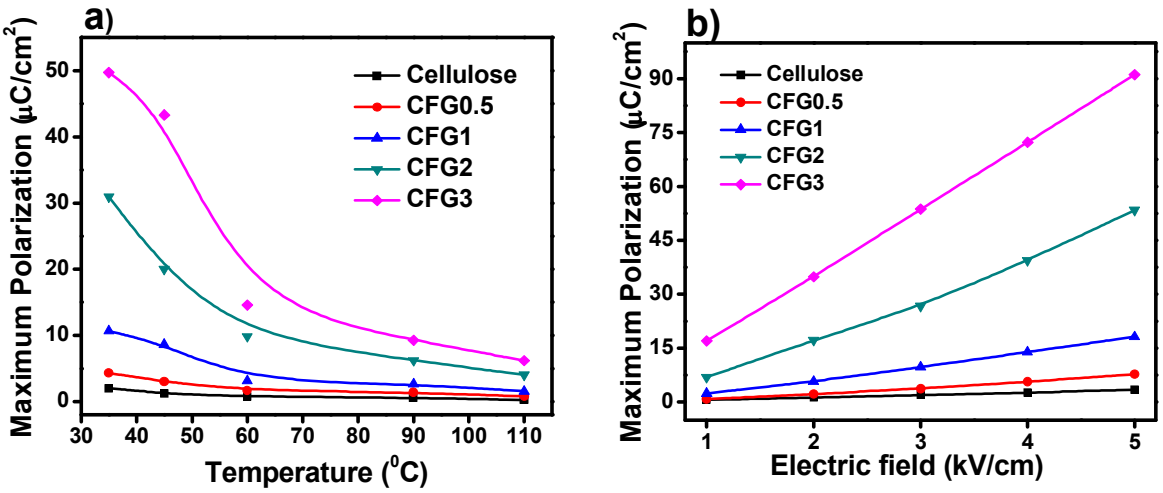

Figure 8: a) Temperature and b) applied field variation of ferroelectric properties of CFG composites and pure cellulose (RH=25% and T= 25 °C)

In the pristine cellulose case, the morphology is rather layer-by-layer and it is possible to trap space charges easily in it [36, 42-44]. As the temperature increases, the trapped space charges play a resistive role against the internal current flow during the relaxation of those charges in the sample. This points out to a fact that the polarization behavior of cellulose nanocomposite is mainly electret-like [36, 45, 46], which has space charge and dipolar polarization under an external electric field at different temperature. With increasing temperature, charges possess much higher energy and they can penetrate deeply into the sample from the electrodes, interacting with dipoles in the nanocomposite, and finally are trapped there. The

higher the temperature, the larger the energy that trapped charges possesses, which make them easier to escape from the trap sites.

In nonconductors the dielectric polarization has two main causes: the electronic (electrons within molecules) and orientation (rotating dipolar molecules or ions changing places) polarizations. While the former has weak temperature dependence, the latter shows strong temperature response. Figure 8b presents the measured polarization–electric field variation between 1 - 5 kV/cm at 1 Hz. An increase of polarization with the applied field for the nanocomposites is observed, whereas for the pristine cellulose less prominent effect is noticed. More clearly the current approaches a steady value in relatively short time with increasing the field strength, i.e. the polarization time is decreasing with increasing the applied field strength. A clear variation of the P–E hysteresis loop for the pristine cellulose and CFG3 is shown in the supplementary Figure S5. When a dielectric layer with electrodes on both sides is subjected to an external electric field, space charge polarization occurs near the electrodes and charges can be trapped inside the material near interfaces while dipolar polarization is generated by internal dipolar elements of the material [46]. As the applied field increases the polarization increases at a given temperature. This behaviour is more prominent in CFG nanocomposites because of more number of dipoles.

In short, the promising level of polarization in the CFG nanocomposites makes them an excellent base material for fabricating advanced ferroelectric materials that could be useful for flexible non-volatile memory cell devices. The resistance of the film depends on the level and duration of the applied voltage and the static current increases with increasing the electric field as usual. This time-dependent absorption current ensures the polarization in the CFG

nanocomposites is due to dipolar orientation and trapping of charge carriers in the bulk whose ejection from the traps will increase with increasing the electric field and temperature. The ferroelectric properties like polarization, coercive voltage, switching period, crystallinity, effect of interfacial layer were also found to be enhanced in the CFG nanocomposites. Moreover, the flexible and renewable behaviors of the CFG nanocomposites are advantageous for implementing flexible and eco-friendly energy storage and electronic devices. Generally, the main difficulty in investigating the behavior of cellulose-based materials in view of its dielectric as well as ferroelectric properties is that it can be easily affected by environmental conditions such as temperature [47]. In our nanocomposites, the functionalizing agent strongly depends on the nanocomposite preparation techniques and other parameters such as dispersion of GO flakes in the cellulose matrix. Thus, the high aspect ratio together with high surface area of the GO fillers allows the formation of high performance energy and memory devices.

Conclusion

Reliable and eco-friendly nanocomposites that can be used for flexible energy and memory storage devices, were fabricated with cellulose grafted GOs. The very smooth and well bind surface in the CFG nanocomposites indicated good reinforcement between GO filler and cellulose matrix and homogeneous dispersion of GO associated with the presence of covalent grafting of GO to cellulose chains. The importance and the role of the temperature and electric field in charge flow process explored the electronic properties of the nanocomposites. The ferroelectric curves of the nanocomposites increased with increase of the applied electric field, indicating the electric field inside the GO fillers is the controlling factor. Based on the hysteresis and polarization behaviours, the possible physical mechanisms of combined capacitive and

resistive polarization in the nanocomposites were understood to be related with desorption/absorption of functional groups in the nanocomposites. The results achieved in this study demonstrated potential applications of the CFG nanocomposites for flexible and eco-friendly energy storage, memory storage and electronic devices.

Acknowledgement This work was supported by National Research Foundation (NRF-2013M3C1A3059586 and NRF-2012R1A2A1A01002087) Republic of Korea.

References

1. J. Kim, S. Yun, and Z. Ounaies, Discovery of Cellulose as a Smart Material, *Macromolecules*, 2006, **39**, 4202-4206.
2. Y. Zhang, Y. Liu, X. Wang, Z. Sun, M. Junkui, T. Wu, F. Xing and J. Gao, Porous graphene oxide/carboxymethyl cellulose monoliths, with high metal ion adsorption, *Carbohyd. Polym.*, 2014, **101**, 392– 400.
3. M.U.M. Patel, N. D. Luong, J. Seppälä, E. Tchernychova and R. Dominko, Low surface area graphene/cellulose composite as a host matrix for lithium sulphur batteries, *J. Power Sources*, 2013, **254**, 55-61.
4. K. K. Sadasivuni, D. Ponnamma, B. Kumar, M. Strankowskie, R. Cardinaels, P. Moldenaers, S. Thomas and Y. Grohens, Dielectric properties of modified graphene oxide filled polyurethane nanocomposites and its correlation with rheology, *Compos. Sci. Technol.*, 2014, **104,** 18–25.
5. H. Grange, C. Bieth, H. Boucher and G. Delapierre, A capacitive humidity sensor with very fast response time and very low hysteresis, *Proc. 2nd Int. Meet. Chemical Sensors, Bordeaux, France*, 1986, 368-371.
6. P. Lian, X. Zhu, S. Liang, Z. Li, W. Yang, and H. Wang, Large reversible capacity of high quality graphene sheets as an anode material for lithium-ion batteries, *Electrochim. Atca*, 2010, **55**, 3909–3914.

7. J. Liu, M. A. G. Namboothiry and D. L. Carroll, Optical geometries for fiber-based organic photovoltaics, *Appl. Phys. Lett.*, 2007, **90**, 133515 (1-3).
8. X. Fan, Z. Z. Chu, F. Z. Wang, C. Zhang, L. Chen, Y. Tang and D. C. Zou, Wire-Shaped Flexible Dye-sensitized Solar Cells, *Adv. Mater.*, 2008, **20**, 592–595.
9. J. H. Kim, S. Mun, H.U. Ko, G. Yun and J. Kim, Disposable chemical sensors and biosensors made on cellulose paper, *Nanotechnol.*, 2014, **25**, 092001(1-9).
10. K. K. Sadasivuni, A.Kafy, L. Zhai, H.U. Ko, S. Mun and J. Kim, Transparent and flexible cellulose nanocrystal/reduced graphene oxide film for proximity sensing, *Small*, 2014, DOI: 10.1002/smll.201402109.
11. K. Y. Choi , H. G. Lim , S. R. Yun , J. Kim and K. S. Kang, The Cause of Nanohole and Nanoparticle Formation on Au-Electrode after Actuation of Electro-Active Paper Actuator*, J. Phys. Chem. C*, 2008, **112**,16204-16208.
12. H. Lin, L. Li, J. Ren, Z. Cai, L. Qiu, Z. Yang and H. Peng, Conducting polymer composite film incorporated with aligned carbon nanotubes for transparent, flexible and efficient supercapacitor, *Sci. Rep.*, 2013, **3**, 1353 (1-6).
13. Z. Niu, P. Luan, Q. Shao, H. Dong, J. Li, J. Chen, D. Zhao, L. Cai, W. Zhou, X. Chen and S. Xie, A "skeleton/skin" strategy for preparing ultrathin free-standing single-walled carbon nanotube/polyaniline films for high performance supercapacitor electrodes, *Energy Environ. Sci.*, 2012, **5**, 8726 -8733.
14. L. Ji, Z. Lin, A. J. Medford and X. Zhang, Porous carbon nanofibers from electrospun polyacrylonitrile/SiO_2 composites as an energy storage material, *Carbon*, 2009, **47**, 3346 – 3354.
15. E. J. Ra, E. Raymundo-Piñero, Y. H. Lee and F. Béguin, High power supercapacitors using polyacrylonitrile-based carbon nanofiber paper, *Carbon*, 2009, **47**, 2984 - 2992.
16. X. Chen, L. Qiu, J. Ren, G. Guan, H. Lin, Z. Zhang, P. Chen, Y. Wang and H. Peng, Novel Electric Double-Layer Capacitor with a Coaxial Fiber Structure, *Adv. Mater.*, 2013, **25**, 6436 - 6441.
17. J. Ren, W. Bai, G. Guan, Y. Zhang and H. Peng, Flexible and Weaveable Capacitor Wire Based on a Carbon Nanocomposite Fiber, *Adv. Mater.*, 2013, **25**, 5965 - 5970.

18. G. Yang, C. Lee, J. Kim, F. Ren and S. J. Pearton, Flexible graphene-based chemical sensors on paper substrates, *Phys. Chem. Chem. Phys.*, 2013, **15**, 1798-1801.
19. Y. Kim, T. K. An, J. Kim, J. Hwang, S. Park, S. Nam, H. Cha, W. Park, J. M. Baik and C. E. Park, A composite of a graphene oxide derivative as a novel sensing layer in an organic field-effect transistor, *J. Mater. Chem.*, 2014, **2**, 4539-4544.
20. D. Ponnamma, Q. Guo, I. Krupa, M. Al-Maadeed, V. K. T., S. Thomas and K. K. Sadasivuni, Graphene and graphitic derivatives filled polymer composites as potential sensors, *Phys. Chem. Chem. Phys*., 2014, DOI: 10.1039/C4CP04418E.
21. N. D. Luong, N. Pahimanolis, U. Hippi, J. T. Korhonen, J. Ruokolainen, L. S. Johansson, J. D. Namd and J. Seppala, Graphene/cellulose nanocomposite paper with high electrical and mechanical performances, *J. Mater. Chem*., 2011, **21**, 13991–13998.
22. K. Gao, Z. Shao, X. Wu, X. Wang, J. Li, Y. Zhang, W. Wang, and F. Wang, Cellulose nanofibers/reduced graphene oxide flexible transparent conductive paper, *Carbohyd. Polym.*, 2013, **97**, 243– 251.
23. W. Ouyang, J. Sun, J. Memon, C. Wang, J. Geng and Y. Huang, Scalable preparation of three-dimensional porous structures of reduced graphene oxide/cellulose composites and their application in supercapacitors, *Carbon*, 2013, **62**, 501-509.
24. J. K. Gregory, D.C. Clary, K. Liu, M. G. Brown and R. J. Saykally, The water dipole moment in water clusters, *Science*, 1997, **275,** 814 – 817.
25. K. K. Sadasivuni, D. Ponnamma, S. Thomas and Y. Grohens, Evolution from graphite to graphene elastomer composites, *Prog. Polym. Sci.*, 2014, **39**, 749-780.
26. D. Ponnamma, K.K. Sadasivuni, M. Strankowski, Q. Guo and S. Thomas, Synergistic effect of multi walled carbon nanotubes and reduced graphene oxides in natural rubber for sensing application, *Soft matter*, 2013, **9**, 10343-10353.
27. K. K. Sadasivuni, M. Castro, A. Saiter, L. Delbreilh, J. F. Feller, S. Thomas and Y. Grohens, Development of poly (isobutylene-co-isoprene)/reduced graphene oxide nanocomposites for barrier, dielectric and sensingapplications, *Mater. Lett.*, 2013, **96**, 109-112.
28. D. Marcano, D. Kosynkin, J. Berlin, A. Sinitskii, Z. Sun, A. Slesarev, L. Alemany, W. Lu and J. Tour, Improved Synthesis of Graphene Oxide, *ACS Nano*, 2010, **4**, 4806–4814.

29. M. Jana, P. Khanra, N. C. Murmu, P. Samanta, J. H. Lee and T. Kuila, Covalent surface modification of chemically derived graphene and its application as supercapacitor electrode material, *Phys. Chem. Chem. Phys.*, 2014, **16**, 7618-7626.
30. S. C. Ray, S. K. Bhunia, A. Saha and N. R. Jana, Electric and ferroelectric behaviour of polymer-coated graphene-oxide thin film, *Physics Procedia,* 2013, **46**, 62 – 70.
31. D. K. Pradhan, R. Choudhary, B. Samantaray, N. Karan, and R. Katiyar, Effect of Plasticizer on Structural and Electrical Properties of Polymer Nanocomposite Electrolytes, *Int. J. Electrochem. Sci.*, 2007, **2**, 861-871.
32. J. K. Yuan, S. H. Yao, Z. M. Dong, A. Sylvestre, M. Genestoux and J. Bai, Giant Dielectric Permittivity Nanocomposites: Realizing True Potential of Pristine Carbon Nanotubes in Polyvinylidene Fluoride Matrix through an Enhanced Interfacial Interaction, *J. Phys. Chem. C*, 2011, **115**, 5515-5521.
33. H. Montès and J. Y. Cavaillè, Secondary dielectric relaxations in dried amorphous cellulose and dextran, *Polymer*, 1999, **40**, 2649 – 2657.
34. E. Whalley and D.D. Klug, Effect of hydrogen bonding on the direction of the dipole-moment derivative of the O–H bond in the water molecule, *J. Chem. Phys.* 1986, **84**, 78 - 80.
35. I. Meric, M. Y. Han, A. F. Young, B. Ozyilmaz, P. Kim and K. L. Shepard, Current saturation in zero-bandgap, top-gated graphene field-effect transistors, *Nat. Nanotechnol.*, 2008, **3**, 654−659.
36. G. Y. Yun, J. H. Kim and J. Kim, Dielectric and polarization behaviour of cellulose electro-active paper (EAPap), *J. Phys. D: Appl. Phys.*, 2009, **42,** 082003 (1-6).
37. A. Abdel-Galil, H.E. Ali, A. Atta and M.R. Balboul, Influence of nanostructured TiO2 additives on some physical characteristics of carboxymethyl cellulose (CMC), *J. Radiat. Res. Appl. Sci.*, 2014, **7**, 36- 43.
38. D. S. Kalika and R. K. Krishnaswamy, Influence of Crystallinity on the Dielectric Relaxation Behavior of poly (ether ether ketone), *Macromolecules*, 1993, **26**, 4252-4261.
39. H. Xu, D. Shen, and Q. Zhang, Structural and ferroelectric response in vinylidene fluoride/trifluoroethylene/hexafluoropropylene terpolymers, *Polymer*, 2007, **48**, 2124-2129.

40. X. Hong, J. Hoffman, A. Posadas, K. Zou, C. H. Ahn and J. Zhu, Unusual resistance hysteresis in n-layer graphene field effect transistors fabricated on ferroelectric Pb.Zr0:2Ti0:8/O3, *Appl. Phys. Lett.,* 2010, **97**, 033114 (1-3)
41. E. B. Song, B. Lian, S. M. Kim, S. Lee, T. K. Chung, M. Wang, C. Zeng, G. Xu, K. Wong, Y. Zhou, H. I. Rasool, D. H. Seo, H. J. Chung, J. Heo, S. Seo and K. L. Wang, Robust bi-stable memory operation in single-layer graphene ferroelectric memory, *Appl. Phys. Lett.*, 2011, **99**, 042109 (1-3).
42. V. F. Petrenko, Electromechanical Phenomena in Ice, Special Report 96-2, US Army Corps of Engineer, 1996.
43. J. F. C. Windmill, A. Zorab, D. J. Bedwell and D. Robert, Nanomechanical and electrical characterization of a new cellular electret sensor–actuator, *Nanotechnol.*, 2008, **19** 035506 (1-7).
44. B. Gross and R. J. D. Moraes, Polarization of the Electret, *J. Chem. Phys.*, 1962, **37,** 710-713.
45. M. Wegener and S. Bauer, Microstorms in cellular polymers: A route to soft piezoelectric transducer materials with engineered macroscopic dipoles, *Chem. Phys. Chem.,* 2005, **6**, 1014 – 1025.
46. M. Goel, Electret sensors, filters and MEMS devices: New challenges in materials research, *Curr. Sci.,* 2003, **85**, 443 – 453.
47. Vincent Ducéré, , Alain Bernès and Colette Lacabanne, A capacitive humidity sensor using cross-linked cellulose acetate butyrate, *Sens. Actuators B: Chem*., 2005, **106**, 331-334.